21, 905 (1993).
13. M. E. MacKay, R. D. Jarrad, G. K. Westbrook, R. D. Hyndman, Shipboard Scientific Party of ODP Leg 146, *ibid.* **22**, 459 (1994).
14. R. Katzman, W. S. Holbrook, C. K. Paull, *J. Geophys. Res.* **99**, 17975 (1994).
15. T. A. Minshull, S. C. Singh, G. K. Westbrook, *ibid.*, p. 4715.
16. S. C. Singh, T. A. Minshull, G. D. Spence, *Science* **260**, 204 (1993).
17. S. C. Singh and T. A. Minshull, *J. Geophys. Res.* **99**, 24221 (1994).
18. R. Matsumoto, C. Paull, P. Wallace, *Init. Rep. Deep Sea Drill. Proj.*, in press.
19. ODP Leg 164 Shipboard Science Party, *Eos* **77**, 219 (1996).
20. We acquired VSP data by firing a 300-cubic-inch (4.9-liter) air gun and recording the shots on a three-component Woods Hole Oceanographic Institution borehole seismometer clamped at 8-m intervals from about 150 to 700 mbsf. Ten to 20 air-gun shots were recorded at each depth and summed to form a stacked section.
21. We perform a weighted, damped, least squares inversion of VSP traveltimes for slowness, minimizing $L = \|T - ZU\| + \mathscr{E}\|P\|$, where T, Z, and U are, respectively, the traveltime, depth, and slowness vectors, P is the second derivative of U, and $\mathscr{E}$ is the Lagrange parameter that governs trade-off between data misfit and model smoothness. We chose $\mathscr{E}$ to be 2.5 to 3.0 for the inversions shown here. The traveltime data cannot resolve thin (<20 m thick) high- or low-velocity layers.
22. J. Korenaga, W. S. Holbrook, S. C. Singh, T. A. Minshull, *J. Geophys. Res.*, in press.
23. M. M. Rowe and J. F. Gettrust, *ibid.* **98**, 463 (1993).
24. Free gas may be produced by several processes: (i) breakdown of hydrate at the BSR as sediment passes downward out of the hydrate stability zone; (ii) in situ biogenic or thermogenic methanogenesis; or (iii) distillation of gas if pore fluid saturated in dissolved methane moves either upward or downward into a region of lower solubility [C. K. Paull, W. Ussler III, W. Borowski, *Ann. N.Y. Acad. Sci.* **715**, 392 (1994)].
25. L. A. Mayer, *Nature* **352**, 148 (1991).
26. S. N. Domenico, *Geophysics* **42**, 1339 (1977); M. N. Toksöz, C. H. Cheng, A. Timur, *ibid.* **41**, 621 (1976).
27. R. Hesse and W. E. Harrison, *Earth Planet. Sci. Lett.* **55**, 453 (1981).
28. J. J. Miller, M. Y. Lee, R. von Huene, *Am. Assoc. Pet. Geol. Bull.* **75**, 910 (1991).
29. M. W. Lee *et al.*, *Mar. Pet. Geol.* **10**, 493 (1993).
30. A weighted mean of the Wood and Wyllie equations [equation 4 of (*29*)] expresses seismic velocity as a function of matrix velocity, porosity, and hydrate content. We used a matrix velocity of 4.37 km/s, water velocity of 1.5 km/s, hydrate velocity of 3.3 km/s, matrix density of 2700 kg/m^3, water density of 1000 kg/m^3, hydrate density of 900 kg/m^3, a weighting factor of 1.0, and porosity values calculated on shipboard samples (*18*). For example, at a depth of 250 mbsf, the shipboard-measured porosity of 60% implies 5% saturation of hydrate to yield a velocity of 1700 m/s.
31. The density of methane in methane hydrate is 123 kg/m^3, calculated from the gram molecular weight of 16 g/mol for methane and 7700 mol/m^3 of hydrate [M. A. Mathews and R. von Huene, *Init. Rep. Deep Sea Drill. Proj.* **84**, 773 (1985)].
32. This value is based on 50% porosity and a density of methane of 200 kg/m^3 at 3200 m below sea level, calculated on the assumption of ideal gas behavior.
33. G. D. Spence, T. A. Minshull, C. Fink, in *Proceedings of the Ocean Drilling Program, Scientific Results (Pt. I)*, B. Carson, G. K. Westbrook, R. J. Musgrave, E. Suess, Eds. (Ocean Drilling Program, College Station, TX, 1995), vol. 146, pp. 163–174.
34. K. A. Kvenvolden and A. Grantz, in *The Arctic Ocean Region*, A. Grantz, L. Johnson, J. F. Sweeney, Eds. (Geological Society of America, Boulder, CO, 1990), pp. 539–549.
35. K. A. Kvenvolden, *Rev. Geophys.* **31**, 173 (1993).
36. We thank the crew of the *Joint Oceanographic Institutions for Deep Earth Sampling Resolution* for their untiring efforts during the drilling and VSP work, especially A. Ribbens, S. Kittredge, K. Kuroki, R. Current, B. Julson, N. Smith, R. Johnson, G. Pollard, and R. Caldow. For enlightening discussions during this work we thank W. Dillon, D. Hutchinson, J. Booth, J. Korenaga, and I. Pecher. Technical assistance ashore was provided by K. Peal, T. Bolmer, R. Busby, S. Rosenblad, M. Gould, and D. Dwyer. We thank the Incorporated Research Institutions for Seismology–Program for Array Seismic Studies of the Continental Lithosphere center at Lamont-Doherty Earth Observatory for loan of Reftek data loggers and software. Supported by JOI-USSAC subaward 7-95 and NSF grant OCE-9504610.

17 May 1996; accepted 12 August 1996

Peculiarities of Methane Clathrate Hydrate Formation and Solid-State Deformation, Including Possible Superheating of Water Ice

Laura A. Stern,* Stephen H. Kirby, William B. Durham

Slow, constant-volume heating of water ice plus methane gas mixtures forms methane clathrate hydrate by a progressive reaction that occurs at the nascent ice/liquid water interface. As this reaction proceeds, the rate of melting of metastable water ice may be suppressed to allow short-lived superheating of ice to at least 276 kelvin. Plastic flow properties measured on clathrate test specimens are significantly different from those of water ice; under nonhydrostatic stress, methane clathrate undergoes extensive strain hardening and a process of solid-state disproportionation or exsolution at conditions well within its conventional hydrostatic stability field.

Gas hydrates, also called clathrate hydrates, are nonstoichiometric compounds with structures consisting of a network of H_2O molecules hydrogen-bonded together like ice and encaging molecules of small-diameter gases. Common natural gas hydrates may have either of two crystal structures, and methane hydrate, $CH_4 \cdot 5.75H_2O$ (ideally), is a structure I hydrate constructed from 46 H_2O molecules with eight cavities available for CH_4 gas molecules. In addition to its possible occurrence on the icy moons of the outer solar system at Saturn and beyond (*1*), methane clathrate occurs on Earth in a variety of geologic settings where CH_4 and H_2O are in chemical contact at low temperature (T) and elevated pressure (P), and possibly harbors the largest untapped reservoir of natural gas on Earth (*2*, *3*). Although discovery of extensive clathrate reservoirs in sediments underlying permafrost regions, deep-oceanic environments, and continental margins and shelves has stimulated recent interest in their formation and recoverability (*4*), many basic physical properties of methane clathrate are poorly known or unmeasured. We have developed a method for fabricating pure aggregates of methane clathrate in quantities suitable for materials testing and have documented anomalous behavior in the formation, stability, and rheology of this compound at elevated P (*5*).

Our objective was to synthesize large-volume, low-porosity, cohesive polycrystalline clathrate aggregates with a uniform fine grain size and random crystallographic grain orientation. Our technique differed from those of previous studies (*6*), most of which involved dynamic conditions of rocking, rotation, or continuous agitation of reaction mixtures, resulting in loose or very porous granular aggregates or strongly textured material unsuitable for physical property measurements. We produced our samples by the reaction $CH_4\ (g) + 6H_2O\ (s \rightarrow l) \rightarrow CH_4 \cdot 6H_2O\ (s)$, by the mixing and subsequent slow, regulated heating of sieved, granular H_2O ice and cold, pressurized CH_4 gas in an approximately constant-volume

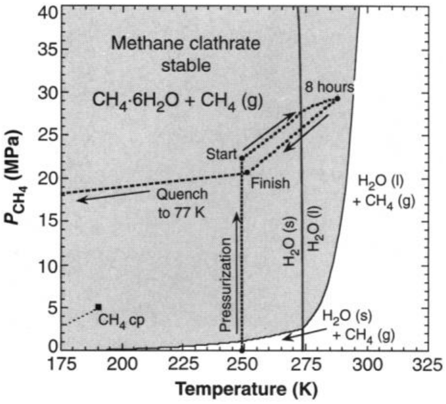

Fig. 1. Phase diagram for the CH_4-H_2O system. Shaded region shows field of methane clathrate stability. At low pressures or high temperatures, clathrate dissociates to H_2O plus CH_4 gas. The metastable extension of the H_2O melting curve is delineated by the gray curve. Dotted lines trace the sample fabrication reaction path.

L. A. Stern and S. H. Kirby, U.S. Geological Survey, Menlo Park, CA 94025, USA.
W. B. Durham, Lawrence Livermore National Laboratory, Livermore, CA 94550, USA.

*To whom correspondence should be addressed.

reaction vessel (7) (Figs. 1 and 2). The initial CH_4 gas P inside the sample vessel was chosen to fill the porosity between the ice grains at a molar ratio of CH_4 to H_2O (seed ice) in the sample vessel in excess of that required for complete reaction (8, 9).

CH_4 P increases almost linearly with T up to 271.5 K with a slope governed primarily by the equilibrium thermal expansion of free CH_4 in the reservoir and sample reaction vessel (Fig. 3A). Initial deviation from this linear relation occurred just above the melting T of H_2O ice, 271.5 K at 27.3 MPa, marking the onset of reaction (Fig. 3A, point A) (10). As time proceeds, the rate of P increase slows as the clathrate-forming reaction consumes much of the vapor phase, producing a measurable offset from the initially linear path. The extent of reaction was determined by this deflection of the P-T slope, and complete reaction produced a P drop (ΔP_r) of 1.8 ± 0.1 MPa (11). The rate of reaction decreased after reaching about 0.5 ΔP_r, and full reaction was most readily achieved by continued heating and self-pressurization of the system to 288 to 289 K and 29.4 ± 0.2 MPa (Fig. 3A, point E). These peak conditions were attained over an interval of 7 to 8 hours after the sample initially crossed the 271.5 K isotherm (Fig. 3A, inset), placing the sample near clathrate dissociation conditions and well above the metastable extension of the H_2O melting curve (Fig. 1).

After complete reaction, samples were cooled to 77 K while venting unreacted CH_4. The resulting samples were shown by x-ray diffraction (XRD) measurements to be pure methane clathrate with no more than trace amounts of H_2O ice (<3%) (Fig. 4). That virtually all the H_2O reacted to form clathrate was also consistent with the calculated molar volume reduction of the reaction (11) and with the lack of a measurable P-T anomaly associated with freezing of unreacted liquid H_2O (Fig. 3A, cooling path). Measurements of the mass uptake of CH_4 in fully reacted samples were consistent with complete reaction of the original H_2O to form clathrate of composition near $CH_4{\cdot}6.1H_2O$ ($\pm 0.1H_2O$), which is the expected equilibrium stoichiometry for this compound at 25 to 30 MPa CH_4 P (11–13). The resulting samples were translucent, white, cohesive aggregates with uniformly fine, equant grains of 200 to 350 μm. All 15 samples produced under these conditions displayed consistent and reproducible run history curves, CH_4 uptake measurements, XRD patterns, and physical appearances. The fully reacted clathrate samples occupy the same cylindrical volume as the starting seed ice, and samples contain 28 to 30% porosity after full reaction (11). This porosity was easily eliminated by externally pressurizing sealed samples while venting the pore space gas, as discussed below.

Curiously, fabrication histories of fully reacted clathrate samples showed no P-T discontinuities associated with bulk melting of the H_2O ice, even though full reaction to form clathrate required many hours at temperatures well above the H_2O melting curve (14). The positive slope of the P-T curve within a few degrees above 271.5 K showed that there was not immediate and complete melting of the ice as it warmed above its liquidus, and the slope of the curve is steeper than would be predicted if all the melt reacted immediately with methane to form clathrate.

This conclusion was verified by control experiments in which neon (Ne), a nonclathrate-forming gas, was used in place of CH_4 under otherwise identical experimental conditions (15). The results (Fig. 3B) confirmed that rapid and complete melting and refreezing of H_2O ice at its melting point occurred in our apparatus when ice was not in the presence of CH_4, and that the associated P-T melting anomalies are easily detectable. The rapid P drop accompanying ice melting (Fig. 3B) was spread out over about 3.5 K as a result of T gradients in the reaction vessel. The T measured by the sample thermocouple lagged the rising T in the surrounding alcohol bath during the P drop (Fig. 3B, inset), a phenomenon that we attribute to the absorption of heat by the endothermic melting of ice. In comparison, the CH_4 runs displayed no such thermal anomalies between sample and bath, indicating that rapid, extensive melting did not occur (16). A P-T discontinuity accompanied refreezing during the cooling phase of the Ne runs, and no net P offset was recorded after returning to the starting conditions (Fig. 3B). Visual inspection and XRD identification of a quenched sample from a Ne experiment showed that it consisted of a clear cylinder of H_2O ice in the bottom half of the mold. The loosely fitting top disk sank to the base of the mold, also indicating full melting of the seed ice. In contrast, fully reacted methane clathrate samples have uniformly granular textures and no displacement of top disks. The Ne control experiments thus demonstrate that all the indicators of equilibrium ice melting expected in our apparatus were observed when a nonclathrate-forming gas was used in the place of CH_4.

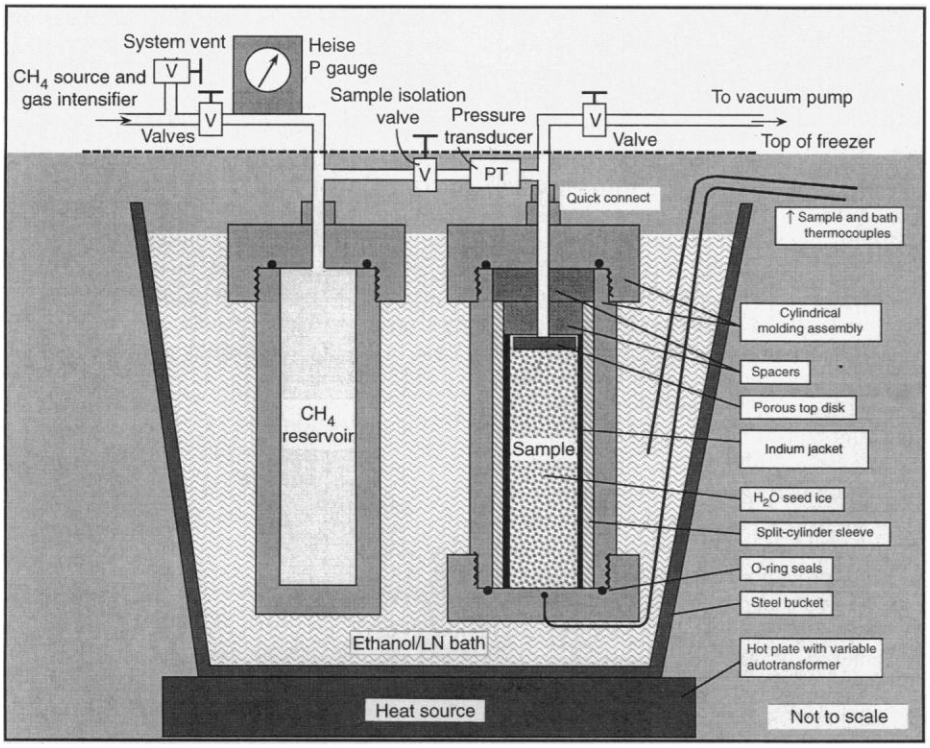

Fig. 2. Apparatus for fabricating cylindrical test specimens of methane clathrate from CH_4 gas and melting ice. The sample assembly is housed in a freezer at 250 K and consists of two vessels immersed in an ethyl alcohol bath. One vessel stores cold, pressurized CH_4 gas at ~35 MPa and 250 K, and the second contains the sample mold with pre-jacketed and pre-evacuated H_2O "seed" ice. Valves allow isolation of any component of the assembly, and a vacuum pump connected to the sample chamber permits evacuation of the system. The sample chamber is warmed by a hot plate situated beneath the alcohol bath and controlled with a variable autotransformer. Temperature is monitored by thermocouples emplaced in the base of the sample mold and in the bath, and pressure is measured by the gauge and transducer. Sample fabrication procedures promoting methane clathrate crystallization are described in the text and in (7).

Three partial-reaction experiments were then conducted on samples of CH_4 + ice, in which the samples were quenched while under pressure at different points along the full reaction curve and subsequently weighed and x-rayed to determine clathrate content as a function of ΔP_r (Fig. 3A, squares B, C, and D). The sample quenched at 0.6 ΔP_r (C) contained 55 ± 5% clathrate, and the sample quenched at 0.8 ΔP_r (D) contained 78 ± 5% clathrate. The third sample was taken to 0.4 ΔP_r (B) and then slowly cooled to 250 K before quenching. That sample showed a measurable *P-T* anomaly upon cooling, indicating that some macroscopic melting had occurred. This result was confirmed by XRD and weight measurements, which showed that the 0.4 ΔP_r sample contained approximately 28 ± 5% clathrate, rather that the predicted 40% if no melt were present. These results suggest that during the early stages of reaction up to about 0.5 ΔP_r, the slow rate of seed ice melting still "outpaces" clathrate formation. After this period, the rate of clathrate formation essentially keeps pace with incipient melting for the remainder of the 8 hours needed for complete reaction under these conditions.

By calculating a hypothetical *P-T* path for melting of the seed ice in the presence of CH_4 gas (*17*), we show that complete melting of ice, with no clathrate formation, would produce a measurable *P* reduction equivalent to 0.26 ΔP_r (Fig. 3A, gray dotted curve). We then calculated the predicted *P* deflection of each partial reaction run for clathrate reaction assuming no melting of unreacted ice, compared to that predicted for complete melting of all residual, unreacted ice (Fig. 3A). The deviation of the observed *P-T* path of the experiments from either the ice-melting curve or the calculated deflections for complete melting of unreacted ice shows that such melting did not occur upon crossing the ice liquidus or up to at least 276 K. Melting may not have been completed until the clathrate reaction was completed near 289 K.

The apparent suppression of the rate of macroscopic ice melting during methane clathrate synthesis raises several questions: Why is complete clathrate reaction achieved only after many hours at temperatures well above the H_2O ice melting point, and why is there no evidence for extensive melting of unreacted seed ice during this time? These questions can be partially answered by considering kinetic parameters such as the induction period, during which hydrate formation is negligible and at the end of which the reaction proceeds at appreciable rates. The induction period needed for methane clathrate formation may be related to the intermediate diameter of the CH_4 molecule with respect to that needed to stabilize either the clathrate structure I or II cavity size, and the consequent retarded formation of critical nuclei for hydrate growth (*2*). A second factor influencing reaction kinetics is the chemical communication of CH_4 with fresh H_2O ice surfaces. For hydrate formation from either solid or liquid H_2O, the formation rate greatly diminishes once a surface layer of hydrate has formed. Vigorous shaking or stirring is needed to renew CH_4 access to the water or ice surfaces to aid the formation process (*18*).

Hydrate growth rates under static conditions were measured by Hwang *et al.* (*9*), in which methane clathrate was grown on disks of melting ice at constant temperatures. Two stages of hydrate formation were observed: an initial "nucleation" period during which the formation rate increased with time, followed by a "growth" period during which the formation rate decayed with time until no more ice remained on the disks. They showed that growth rates were determined by the rate of supply of the hydrate-forming species to the growth surface, as well as the rate of removal of the exothermic heat of formation from the surface (*19*). The onset of ice melting along exposed surfaces promoted clathrate formation by providing both a "template" for the formation of hydrates and a heat sink for absorbing the heat of formation during clathrate growth. Our observations generally agree with these interpretations of Hwang *et al.* (*9*). We further conclude from sample textures and run records that the

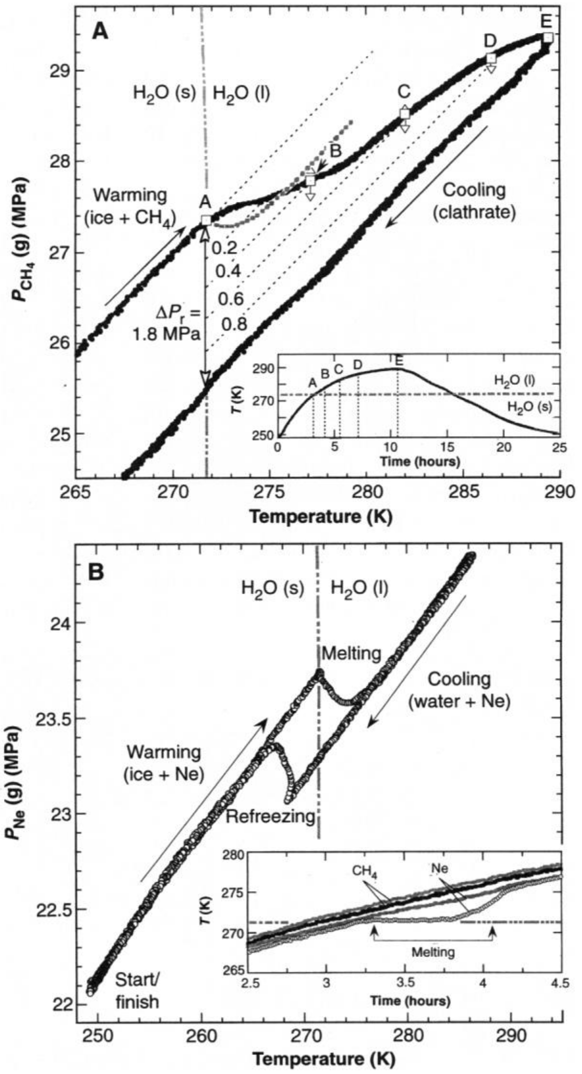

Fig. 3. (**A**) Pressure-temperature (*P-T*) history of sample fabrication conditions promoting the clathrate-forming reaction CH_4 (g) + H_2O (ice) → $CH_4{\cdot}6H_2O$. Reaction initiates just above the H_2O solidus but slows substantially after ~50%, perhaps as a result of "armoring" effect (see text). Full reaction is achieved by steadily increasing *T* and is accompanied by a 1.8-MPa pressure reduction (ΔP_r). Persistence of metastable (superheated) ice is inferred by the lack of a *P-T* discontinuity in the reaction path upon crossing the ice melting curve at A. In comparison, the predicted *P-T* path for full melting of all seed ice with no clathrate formation is shown by the gray dotted curve. Partial-reaction experiments (open squares) that were quenched after reaching the specific fractions of ΔP_r—0 (A), 0.4 (B), 0.6 (C), 0.8 (D), and 1.0 (E)—contained 0, 28, 55, 78, and 100% (±5%) methane clathrate, respectively. Triangles and inverted triangles show the calculated positions associated with no melting and full melting, respectively, of all unreacted ice in each partially reacted sample. That the observed curve does not pass through these positions indicates that whereas some melt accumulates during reaction, complete melting of all unreacted ice is not occurring. (**Inset**) Temperature-time (*T-t*) profile shows that 7 to 8 hours are required for full reaction from A to E at these *P-T* conditions. (**B**) *P-T* record of control experiment with Ne gas + H_2O ice demonstrates that full melting and refreezing of H_2O ice occurs near its solidus when in the presence of nonhydrate-forming gas. (**Inset**) Detail of *T-t* history of Ne (g) + H_2O ice in the region of ice melting, showing the lag of the sample *T* (open circles) compared with the bath *T* (gray trace) associated with the absorption of heat by the endothermic melting of ice (*15*). No such effect is displayed by the thermal history of the methane clathrate run, also shown (clathrate sample *T* is black trace, bath *T* is adjacent gray line).

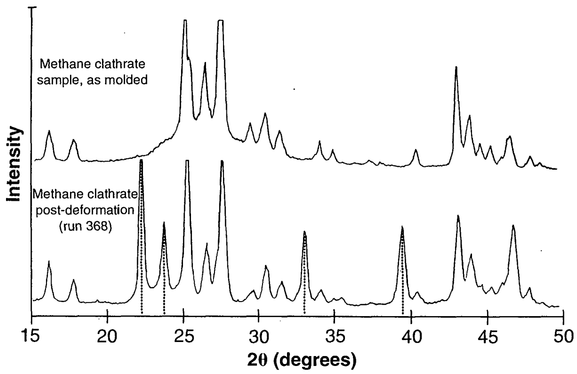

Fig. 4. X-ray powder diffraction (XRD) patterns for methane clathrate as grown (top) and after mechanical testing (bottom). Methane clathrate deformed under nonhydrostatic stress undergoes a partial solid-state disproportionation, as evidenced by H_2O ice peaks (dotted lines) found in post-deformation XRD patterns.

superficial layer of hydrate enveloping each seed ice grain not only rate-limits reaction in the grain interiors, but may also effectively "armor" the grain from nucleating melt and consequently suppress the rate of melting of ice grains. Once such a rind of hydrate has encased an ice grain, the most likely process of continued clathrate formation involves solid-state diffusion of CH_4 gas to the ice core (*20*).

The slope of the *P*-*T* path during clathrate synthesis experiments does not change abruptly upon crossing the ice melting curve (Fig. 3A), and there is a period of several tens of minutes during which little clathrate formation or ice melting appears. These results suggest that melting of the ice grains may be inhibited before the growth of a substantial hydrate layer (*21*). It can be argued that melting should not occur because the only equilibrium phases are methane gas and clathrate (Fig. 1), but over the 8-hour duration of reaction, it is reasonable to assume that equilibrium conditions did not prevail within hydrate-encased grains because of insufficient access of CH_4 to grain interiors. We would expect, therefore, to see evidence of bulk melting as the grain interiors melt before complete reaction. Because we see little or no evidence for either melting or clathrate formation early in the experiment above the ice melting point, we conclude that the armoring effect serves mainly to perpetuate the inhibition of ice melting and its metastable persistence (*22*).

Although the superheating of ice under clathrate-forming conditions seems implausible, we are unable to find a satisfactory alternative explanation for our observations (*23*). One possibility is that early-forming clathrate encased and sealed the ice grains and prevented pressure reductions associated with ice melting inside them from communicating with the CH_4 gas occupying the porosity and, in turn, with our gas pressure measurement system. This explanation seems unlikely because the departure of the *P*-*T* path from that expected for ice melting is prominent at temperatures just above the onset of reaction (Fig. 3A) and would require that strong clathrate pressure seals form around the ice grains during initial reaction, when the clathrate layer would be thin and presumably weak. Moreover, the hydrate shell would need to have nearly zero thermal conductance because no thermal lag associated with the absorption of heat by endothermic melting was observed during heating above 271.5 K (Fig. 3B, inset). We have not, however, verified the existence of such superheated ice by measuring or experimenting with its physical property characteristics.

The strengths of seven methane clathrate specimens were subsequently measured in constant–strain rate compression tests in a triaxial gas deformation apparatus, with N_2 or He gas as the confining medium (*24*, *25*). The thin, soft jackets of indium in which the samples were grown served to exclude the pressure medium and were later used for examination of deformation microstructures replicated from the outer sample surface.

Before deformation, clathrate samples were hydrostatically pressurized and compacted in the apparatus at 170 K (*26*). One sample (366, Table 1) was quenched after compaction and examined in its undeformed state. Volumetric measurements showed that essentially all porosity was eliminated and that a cylindrical sample shape was maintained with only minor distortion. XRD analysis revealed the presence of a small amount of H_2O ice in the sample, estimated at 7 ± 2 volume %. This ice is likely produced by solid-state disproportionation of clathrate, because increasing *P* changes clathrate stoichiometry from $CH_4{\cdot}6.1H_2O$ to $CH_4{\cdot}5.8H_2O$ (*12*). Such a pressure-induced unmixing process would precipitate the approximate volume fraction of ice detected in the x-ray patterns.

Strength measurements were then performed at conditions ranging from 140 to 200 K, 50 to 100 MPa, and $\dot{\varepsilon} = 3.5 \times 10^{-4}$ to 3.5×10^{-6} s^{-1} (Table 1 and Fig. 5). Test results revealed that methane clathrate has a measurably different steady-state strength than H_2O ice, and that the strength of

Table 1. Mechanical test conditions and results. P_c, confining pressure with N_2 or He gas medium; ε_t, total strain; σ_y, yield strength; and σ_{ss}, steady-state strength.

Run no.	Step	*T* (K)	P_c (MPa)	$\dot{\varepsilon}$ (s^{-1})	ε_t	σ_y (MPa)	σ_{ss} (MPa)	Comments
281	1	160	59	3.5×10^{-4}	0.125	–	>85	Strain hardening
	2	160	50	3.5×10^{-6}	0.150	–	60	Strain hardening
	3	160	50	3.5×10^{-4}	0.160	100	–	Brittle failure; ≈25% ice post-deformation*
282	1	140	50	3.5×10^{-6}	–	71	–	Failure, multiple events
	2	140	50	3.5×10^{-4}	0.160	94	–	Failure, multiple events; 25% ice
366	1	168	100	–	–	–	–	Pressurization and compaction only†; 5 to 10% H_2O ice after compaction
367	1	185	100	3.5×10^{-5}	0.138	–	71	Strain hardening at 10^{-5} step only
	2	185	100	3.5×10^{-4}	0.215	96	90	≈30% H_2O ice post-deformation
368	1	168	100	3.5×10^{-5}	0.185	–	102	Strain hardening; 25% ice
369	1	168	100	3.5×10^{-5}	0.16	–	100	Identical run as 368 with gas collection; system emplaced; no evolved CH_4 gas‡
370	1	200	100	3.5×10^{-5}	0.120	–	62	Strain hardening at 10^{-5}; no evolved gas‡;
	2	200	100	3.5×10^{-4}	0.230	85	80	≈30% ice post-deformation

*All samples were analyzed pre- and post-deformation by powder XRD. †Samples 367, 368, 369, and 370 all underwent identical pressurization and compaction as 366 before testing. ‡Runs 369 and 370 had a gas collection system attached throughout testing to detect evolved CH_4 gas.

clathrate appears to be less T-sensitive than ice (Fig. 5A). Moreover, the characteristics of transient deformation were markedly different (Fig. 5B). Whereas H_2O ice typically exhibits a strength maximum before leveling off to steady flow stress, usually within the first 5 to 10% of strain, methane clathrate exhibits monotonic strain hardening drawn out over the first 15% or more of strain.

Comparison of pre- and postdeformation XRD analyses shows that the samples underwent further structural changes while deforming within the clathrate stability field. XRD peak intensities of the deformed samples suggest that 25 ± 10 volume % ice precipitated during deformation, compared with <3% ice in the x-ray patterns of as-grown clathrate (Fig. 4) and 7% ice in the pressurized-only sample. It is possible, however, that heterogeneous ice precipitation or deformation-enhanced textural and grain size changes in the precipitated ice increased the apparent ice peak intensities (*27*). No peaks were observed in postdeformation x-ray patterns to indicate growth of any other phase besides ice and structure I methane clathrate. After first detecting this apparent solid-state disproportionation of the clathrate, we attached a gas collection system to the vent line for two of the runs to observe and collect possible CH_4 gas evolving during deformation. The only gas that vented, however, was that squeezed from the pores during initial pressurization before deformation. No gas evolved from the system during any portion of deformation testing or subsequent unloading. Although collapse of the clathrate structure could occur if as-molded material were strongly nonstoichiometric and hence contained significant gas molecule vacancies, this is unlikely because we measured full uptake of CH_4 gas into the as-molded material. We therefore conclude that at the deformation conditions of this study, methane clathrate apparently undergoes a form of stress-enhanced exsolution or precipitation within its nominal P-T field of thermodynamic stability.

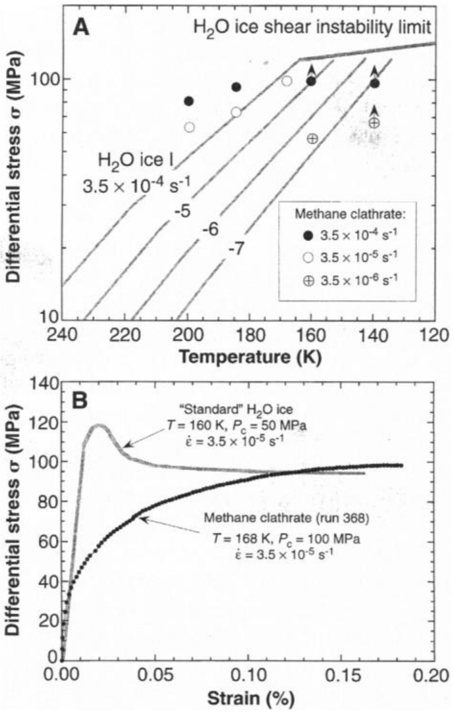

Fig. 5. (**A**) Variation of strength with temperature for methane clathrate, showing measurably different strength than H_2O ice I. H_2O ice flow law relations are from (*25*). Clathrate data points with arrows indicate faulting behavior. (**B**). Stress-strain curves of deformed methane clathrate (run 368) showing systematic strain hardening, compared with the sharp yielding, strain softening, and steady-state flow of "standard" polycrystalline H_2O ice.

Over the time scales of our experiments, the CH_4-H_2O system exhibits several peculiar features, including the metastability of ice + CH_4 mixtures both below and above the H_2O liquidus line and the prominent solid-state precipitation of ice from deformed polycrystalline methane clathrate within the nominal stability field of the clathrate. Although the time scales of clathrate growth and ice precipitation probably differ from those of other clathrate environments, the peculiarities we observed may have relevance to the growth and stability of methane clathrate in terrestrial permafrost and marine sediments and in the outer solar system. We describe here a simple method for growing dense, polycrystalline methane clathrate suitable for material testing, a development that should aid subsequent investigations of its growth and physical properties.

REFERENCES AND NOTES

1. S. Miller, *Proc. Natl. Acad. Sci. U.S.A.* **47**, 1798 (1961); G. Consolmagno, *J. Chem. Phys.* **87**, 4202 (1983); D. Cruikshank, R. Brown, R. Clark, in *Ices in the Solar System*, J. Klinger *et al.*, Eds. (Reidel, Dordrecht, The Netherlands, 1985), pp. 817–827; R. G. Prinn and B. Fegley Jr., in *Origin and Evolution of Planetary and Satellite Atmospheres*, S. K. Atreya *et al.*, Eds. (Univ. of Arizona Press, Tucson, AZ, 1989), pp. 78–136; J. Lunine and D. Stevenson, *Astrophys. J. Suppl.* **58**, 493 (1985).
2. E. Sloan, *Clathrate Hydrates of Natural Gases* (Dekker, New York, 1990).
3. K. Kvenvolden, *Chem. Geol.* **71**, 41 (1988).
4. Because hydrates concentrate CH_4 by a factor of 165 with respect to standard temperature and pressure gas and as little as 10% of the recovered energy is required for dissociation, hydrate reservoirs are considered a substantial future energy resource; the total amount of gas in this solid form may surpass the energy content of the total fossil fuel reserves by as much as a factor of 2 [(*2*, *3*); G. Claypool and I. Kaplan, in *Natural Gases in Marine Sediments*, I. Kaplan, Ed. (Plenum, New York, 1974), pp. 99–139].
5. L. Stern, S. Kirby, W. Durham, *Lunar Planet. Sci. Conf. XXVII* (abstr.), p. 1271 (1996); W. Durham, S. Kirby, L. Stern, in *Solar System Ices*, B. Schmitt, Ed., in press.
6. R. Barrer and D. Ruzicka, *Trans. Faraday Soc.* **58**, 2253 (1962); R. Barrer and A. Edge, *Proc. R. Soc. London Ser. A* **300**, 1 (1967); B. Falabella and M. Vanpee, *Ind. Eng. Chem. Fundam.* **13**, 228 (1974); K. Aoyogi, K. Song, R. Kobayashi, E. Sloan, P. Dharmawardhana, *Gas Processors Assoc. Res. Rep. No. 45* (Tulsa, OK, 1980); see (*2*) for review of fabrication techniques.
7. CH_4 gas from a source tank is initially boosted in P by a gas intensifier and routed into sample molding vessels housed in a deep freezer. The sample assembly (Fig. 2) consists of two steel vessels immersed in an ethyl alcohol bath initially held at freezer T (~250 K); one vessel serves as a reservoir to store and chill the pressurized CH_4 gas, and the other houses the sample mold. The mold consists of a hollow split-cylinder that encases an indium sleeve filled with 26 g of sieved 180- to 250-μm H_2O ice seed grains made from triply distilled H_2O and packed to a controlled 40% porosity. Initially, the sample chamber with seed ice is closed off from the reservoir, evacuated, and then isolated from the vacuum pump. A loosely fitting top disk inserted on top of the packed seed ice grains prevents displacement of the packed ice grains during evacuation. The reservoir vessel is first charged with pressurized CH_4 to 34 MPa, and cools to freezer T. The reservoir is then opened to the pre-evacuated sample chamber, and CH_4 P equilibrates to roughly 22 MPa throughout the assembly. The bath T is then slowly raised by means of the hot plate beneath the alcohol bath (at the rate shown in Fig. 3A, inset), and as the mold and reservoir warm, they self-pressurize. P increases steadily with T until reaction initiates, at which point consumption of CH_4 gas by clathrate formation slows the rate of P increase. A data-acquisition system was used to monitor and record T and P conditions throughout each run, and the extent of reaction was determined by the measured P-T offset from the CH_4 expansion curve. After full reaction is reached, the heat source is turned off and the system slowly cools to 250 K. The sample chamber is then quenched in liquid N_2, isolated from the reservoir, vented, disconnected from the apparatus, and opened. The inner, hollow split-cylinder containing the sample is pushed from the mold and pried off the jacketed sample. The jacketed samples are stored in liquid N_2 until mechanical testing.
8. Hwang *et al.* (*9*) note that a high-P driving force is required for measurable clathrate formation rates, and their experiments verified that for clathrate formation from melting ice, higher gas P yielded higher formation rates. Makogon (*20*) had earlier suggested that as hydrate formation is an interfacial process, high concentrations of hydrate-forming species are required at the interface.
9. M. Hwang, D. Wright, A. Kapur, G. Holder, *J. Inclusion Phenom.* **8**, 103 (1990).
10. XRD patterns of samples from previous runs with maximum temperatures below the H_2O liquidus showed no evidence of clathrate formation, as expected on the basis of previous investigations (*6*, *9*), and no deflections were observed in the P records to indicate any significant CH_4 uptake. Samples from previous experiments taken to 273 to 280 K for 4 to 6 hours showed only partial reaction, with roughly equal fractions of clathrate and ice in their XRD patterns.
11. The volume of an empty structure I clathrate lattice is 16% greater than that of an equivalent mass of ice I, regardless of stoichiometry [the empty structure I lattice has a density of 0.78 g/cm^3, and stoichiometric methane clathrate has a density near that of ice (0.90 g/cm^3 versus 0.92 g/cm^3 for ice)], but there is a large, $-\Delta V$ associated with clathrate formation due to the volume reduction of the gas phase into the clathrate structure. At our test conditions, the ΔV of reaction is −21%. We start with 26 g of seed ice, and the actual molar reaction promoted is $1.4H_2O + 0.23CH_4$ (gas) $\rightarrow 0.23(CH_4{\cdot}6.1H_2O)$. The 3.8 g of methane uptake measured after sample synthesis confirms this stoichiometry and is consistent with (*12*). ΔP_r measured during synthesis is only a 6.4% drop from the starting P, due to the large volume of the gas reservoir that is open to the system throughout synthesis.
12. Gas hydrate number n varies with P; increasing P maximizes guest-molecule site occupancy. At sample synthesis conditions (~28 MPa) the hydrate number n for methane clathrate should be 6.1 ± 0.1, and at 100 MPa n = 5.85 ± 0.05 [S. Saito, D.

Marshall, R. Kobayashi, *Am. Inst. Chem. Eng. J.* **10**, 734 (1964); also see (*13*), p. 54.]

13. *Handbook of Gas Hydrate Properties and Occurrence* (U.S. Dept. of Energy Publication DOE/MC/19239-1546, 1983).
14. Exceptions were those samples that leaked *P* at warm *T* to either prevent full reaction or to cause partial dissociation of clathrate to CH_4 gas + H_2O liquid. After refreezing, these samples showed obvious melt textures; they displayed an outer cylindrical ring of clear, nonporous ice, with cloudy, gas-charged ice concentrated in the center of the sample as the freezing front progressed from the outside to the interior. Partially dissociated samples also showed large amounts of ice in their XRD patterns. Additional evidence of melting was provided by the loosely fitting top disk (Fig. 2). In samples that leaked *P*, the disk was found to drop to a midpoint in the molding tube as residual seed ice melted. In fully reacted samples, however, the disk remained at the top of the sample.
15. Only H_2, He, and Ne are too small to form clathrates at our test conditions; we chose Ne because it is the largest of these and hence the easiest to seal.
16. The clathrate-forming reaction CH_4 (g) + $6H_2O$ (ice) → $CH_4{\cdot}6H_2O$ liberates a small amount of latent heat {~20 ± 0.3 kJ/mol at 273 K and a CH_4 pressure of 28 MPa, as determined from the Clapeyron slope [T. Makogon and E. Sloan, *J. Chem. Eng. Data* **39**, 2, 351 (1994)], the measured enthalpy of formation at standard conditions [Y. Handa, *Chem. Thermodyn.* **18**, 915 (1986)], the reaction volume change (*11*), and its variation with pressure (*13*)}. This heat is not reflected as a sample *T* anomaly (Fig. 3B, inset), evidently because the clathrate reaction occurs over 8 hours and such heat would be small compared with the exchange of heat by conduction of the sample with its surroundings. The standard enthalpy for melting H_2O ice is −6.01 kJ/mol, or −36.07 kJ/6.1 mol for comparison with the clathrate-forming reaction.
17. This curve was calculated from the melting behavior of ice measured in Ne runs and assumes that (i) the seed ice grains melted as the ice did in the Ne run, (ii) changes in CH_4 *P* scale with Ne *P* changes through the Ne and CH_4 equations of state, and (iii) solubility of Ne in H_2O is negligible. The magnitude of the *P* drop was verified independently from the CH_4 equation of state.
18. P. Villard, *C. R. Assoc. Fr. Avanc. Sci.* **106**, 1602 (1888). See also (*2*, *9*).
19. Hwang *et al.* (*9*) note that because hydrate formation is an exothermic process, heat released by the phase change during crystallization increases the *T* at the formation interface. This effect is greater for hydrate formation from liquid H_2O than from ice because the heat of formation is partially absorbed by the melting ice.
20. Conceptual models of hydrate growth by diffusion have been discussed previously [Y. Makogon, *Hydrates of Natural Gases*, W. H. Cielewicz, Transl. (PennWell, Tulsa, OK, 1981)] and later by Hwang *et al.* (*9*).
21. Superheating has been measured in gold-plated silver single crystals [J. Daeges, H. Gleiter, J. Perepezko, *Phys. Lett.* **119A**, 79 (1986)], and results suggest that either a free external surface or internal defects or dislocations are critical for melting to take place at the normal melting point [S. Phillpot, J. Lutsko, D. Wolf, S. Yip, *Phys. Rev. B* **40**, 2831 (1989); see also S. Phillpot, S. Yip, D. Wolf, *Comput. Phys.* **3**, 20 (1989). In the present study, we detected no clathrate formation during the initial *T* run-up to 271.5 K (*10*), when the sample is in the ice sub-solidus field, and hence we have ruled out the liklihood that a rind of clathrate encased the ice grains before they were warmed above the H_2O liquidus. It remains possible, however, that such a microlayer actually formed but was at or below our XRD detection levels.
22. Also, methane hydrate crystallization from a bulk liquid H_2O phase is difficult to initiate because of the low solubility of the gas in the bulk liquid (*2*, *9*).
23. Several investigators have reported demonstrating the phenomenon of superheating ice with respect to the vapor phase [E. Roedder, *Science* **155**, 1413 (1967); G. Schubert and R. E. Lingenfelter, *ibid.* **168**, 469 (1970); see also discussion by B. Kamb, *ibid.* **169**, 1343 (1970)] or with respect to the liquid phase, M. Kåss and S. Magun [*Z. Kristallogr.* **116**, 354 (1961)]. See also C. Knight and A. DeVries, *Science* **245**, 505 (1989).
24. H. Heard, W. Durham, C. Boro, S. Kirby, in *The Brittle-Ductile Transition in Rocks, Geophysical Monograph* 56, A. Duba *et al.*, Eds. (American Geophysical Union, Washington, DC, 1990), pp. 225–228. In our experiments, piston force and displacement rate were recorded, corrected for instantaneous sample area and length changes, and converted to differential stress (σ), axial shortening strain (ε), and strain rate ($\dot{\varepsilon}$).
25. W. Durham, S. Kirby, L. Stern, *J. Geophys. Res.* **97**, E12, 20883 (1992); S. Kirby, W. Durham, M. Beeman, H. Heard, M. Daley, *J. Phys.* **48** (suppl.), 227 (1987).
26. During hydrostatic compaction, confining *P* was slowly "stepped" up to 100 MPa in increments of about 20 MPa. After each *P* step, the piston was advanced to touch and square the bottom of the sample, then advanced just sufficiently to lightly compress the sample in order to compact it with minimal plastic deformation. Six of the samples were compacted by means of an internal vent line to eliminate the pore-space gas, and two of the samples were compacted without the venting capability. The two nonvented samples (281 and 282; Table 1) showed equally large fractions of ice in their post-deformation x-ray patterns as the vented samples.
27. Indium jacket replicas of deformed sample surfaces showed evidence of heterogeneous ice precipitation. Areas with exsolved ice appear on jackets of all deformed samples as discrete patches with noticeably finer grain size than the surrounding clathrate.
28. We thank B. Kamb, J. Kargel, K. Kvenvolden, and W. McKinnon for critically reviewing the manuscript and for helpful discussions. This work was supported under NASA order W-18,927 and was performed in part under the auspices of the U.S. Department of Energy by the Lawrence Livermore National Laboratory under contract W-7405-ENG-48.

29 April 1996; accepted 10 July 1996

A Trinuclear Intermediate in the Copper-Mediated Reduction of O_2: Four Electrons from Three Coppers

Adam P. Cole, David E. Root, Pulakesh Mukherjee,
Edward I. Solomon, T. D. P. Stack*

The reaction of metal complexes with dioxygen (O_2) generally proceeds in 1:1, 2:1, or 4:1 (metal:O_2) stoichiometry. A discrete, structurally characterized 3:1 product is presented. This mixed-valence trinuclear copper cluster, which contains copper in the highly oxidized trivalent oxidation state, exhibits O_2 bond scission and intriguing structural, spectroscopic, and redox properties. The relevance of this synthetic complex to the reduction of O_2 at the trinuclear active sites of multicopper oxidases is discussed.

The copper-mediated activation of O_2 plays a vital role in biological and synthetic oxidative catalysis (*1*–*4*). Recent investigations of O_2 reduction with Cu(I) complexes have shown that Cu is remarkably versatile regarding both the degree of reduction and the coordination mode of the reduced O_2 species. Reductions to superoxide (*2*, *5*), peroxide (*2*, *3*, *6*, *7*), and water (*2*) involving one, two, and four electrons (e^-), respectively, have been documented, in which each Cu(I) supplies one electron. The variety of Cu sites found in natural enzymes that bind or activate O_2 reflects this versatility. The Cu enzymes responsible for the $4e^-$ reduction of O_2 to H_2O—laccase, ceruloplasmin, and ascorbate oxidase—each contain a trinuclear Cu active site (*8*–*12*) with an additional mononuclear "blue" Cu site 12 Å distant (*9*). The known binuclear Cu proteins hemocyanin and tyrosinase (*3*, *6*) bind O_2 through $2e^-$ reduction to $O_2{}^{2-}$, but the fully reduced trinuclear site is the minimal structural subunit required for biological O_2 bond cleavage and reduction to H_2O (*8*, *13*).

A self-assembly approach to the synthesis of a bi- or trinuclear Cu-O_2 cluster from monomeric Cu(I) complexes and O_2 assumes facile assembly and thermodynamic stability of the resulting product under the reaction conditions. Accordingly, the use of simple ligands is an appropriate strategy. A number of monomeric 1:1 Cu(I):*N*-peralkylated-diamine complexes were examined by manometry for 3:1 Cu:O_2 reactivity. Structural and spectroscopic studies of the oxidation of one such Cu(I) complex (**1**) demonstrate the formation of a trinuclear intermediate (**2**) in the Cu(I)-mediated reduction of O_2 whose 3:1 stoichiometry is unprecedented not only in the case of Cu but among all discrete metal-O_2 reactions (Scheme 1, Me = methyl). Its structural, spectroscopic, and redox properties indicate that, in the process of O_2 bond cleavage, the three Cu(I) sites in **2** are oxidized by a total of four electrons, forming a mixed-valence cluster with bridging oxide ligands that stabilize one of the Cu sites in its normally inaccessible

---

Department of Chemistry, Stanford University, Stanford, CA 94305, USA.

*To whom correspondence should be addressed.